A basic study on admittance control using torsional torque control for a two-inertia system

1st Takaaki Hayashi
Graduate School of Engineering
The University of Tokyo
Chiba, Japan
hayashi.takaaki21@ae.k.u-tokyo.ac.jp

2nd Shota Yamada
Graduate School of Engineering
The University of Tokyo
Chiba, Japan
yamada.s@edu.k.u-tokyo.ac.jp

3rd Hiroshi Fujimoto
Graduate School of Engineering
The University of Tokyo
Chiba, Japan
fujimoto@k.u-tokyo.ac.jp

***Abstract*—Demand for cooperative robots is increasing. One of their control methods is admittance control. Not many studies worked on admittance control for a plant with resonance. We aimed at designing the control system so that the whole system does not vibrate at the anti-resonance frequency of the plant. The admittance control was attributed to the torsional torque control. The effectiveness of the proposed method in vibration due to a dynamics of a two-inertia system was validated in the simulations and experiments, especially by the result of time response that showed the reduction of the overshoot by more than $30\,\%$.**

***Index Terms*—Admittance control, Vibration suppression, Torsional control, Two-inertia system, Human-robot interaction**

I. Introduction

In recent years, human-robot interactions have received increasing attention. Especially in industry, the demand for cooperative robots that share a workspace with humans and work in cooperation with humans is increasing, and research on those kinds of robots has been conducted [1]. Due to the increasingly shrinking working population, labor force supplementation has been increasingly necessary. In addition, to meet the increasing diverse needs of customers, high-mix low-volume production rather than small variety mass production has come to be demanded. Therefore, collaborative robots, as shown in Fig. 1, are becoming necessary that can reduce the number of workers performing tasks and that can manufacture to meet diverse needs. When a human tried to move a conventional industrial robot from the outside, such as the robot ' s arm or leg, a great deal of force was required. Therefore, for example, the burden on skilled technicians to directly teach the work operation to the robot was significant. It is important to allow robots to move easily with less force for better interaction between humans and robots. In this paper,

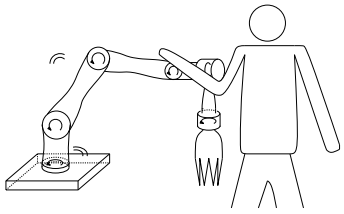

Fig. 1. Human-robot collaboration: a robot need to be friendly to human.

the magnitude of the load-side angular velocity relative to the torque applied by the human when the robot is moved from the outside is called backdrivability. The higher the backdrivability of robots is, the smaller the force to move the robots by humans is. Inertia and friction on the drive side are greatly amplified to be transmitted to the load side at a high reduction ratio. When the reduction ratio is small, the amplified frictions are small. In that case, however, the output torque at the same load-side angular velocity is small and may not meet the output torque required for the work.

Methods to improve backdrivability have been actively studied in recent years. They include hardware and software approaches. Research, such as [2] is hardware approaches. However, these hardware approaches have drawbacks, such as reduced robot rigidity and comparative difficulty of implementation on current robots. One of the software approaches is friction compensation [3] [4]. They need complicated parameter identification for complex friction models or have difficulty in being used with other controls. Some studies aim to reduce the torque transmitted to the load side to 0 by control [5] [6] [7]. Torsional torque controls or angular transmission error controls are used. In these controls, the goal is to make the system feel as if it were only on the load side to humans and the environment. Some studies aim to assist the load not only aims to remove dynamics other than the load side. In paper [8], how backdrivable the whole system is can be specified with one parameter. This means the degree of freedom to specify is small. In paper [9], the backlash was assisted by compensating for the backlash. In this method, the transfer function from the human torque to the load-side angular velocity in the entire system is uniquely determined, and the desired physical parameters such as inertia and viscosity cannot be specified. As an assistant control that achieves the desired physical parameters, there is admittance control [10]. This method converts human torque into angular velocity commands and controls them, enabling intuitive assistance. Recent studies include those that adaptively determine admittance parameters [11] [12] and those that make structural innovations [13] [14], among others. In designing these controls, there are many papers that consider the joint as a rigid body. When flexible reducers such as strain wave gears are used, anti-resonance and resonance exist at low frequencies, and vibrations caused

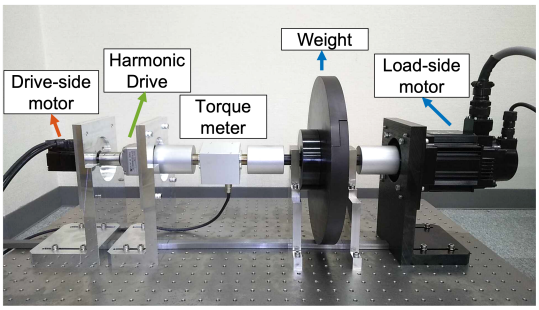

Fig. 2. The experimental setup.

by them can occur on the load side. However, not so much research takes into consideration the dynamics of joint with resonance. Although [15] evaluated the performance of the control system for a plant with resonance, it did not consider the resonance positively in designing the control system. [16] and [17] considered the resonance in designing the control system, and proposed the designing procedures. However, collocated information may not be effectively utilized in these works. The contributions of this paper are as follows:

1) Showing the superiority of torsional torque feedback in admittance control of a two-inertia system
2) Proposal for a filter which attributes admittance control to torsional torque control
3) Validation of the above in an experiment

This paper is organized as follows. In section 2, the properties of the experimental setup including the structure and the modeling are described. In section 3, the method of the conventional admittance control and that of the proposed one are described. In sections 4 and 5, the conditions and the results of the simulations and the experiments are described. Finally, in section 6, the conclusion and future work are described.

II. Modeling of the Experimental Setup

The experimental setup used in this paper is shown in Fig. 2. The main components are a motor on the drive side (SGM7J-01A6A21), a strain wave gear (Harmonic Drive (CSF-14-50-1U)), a motor on the load side (SGM7A20A6A21), and a weight. The setup is a model of a robot joint. The torque applied by the load-side motor is regarded as the torque applied by a human to the robot from outside in this paper. The weight is designed to meet the condition where the output-side inertia is about four times as input-side inertia, which is common in collaborative robots.

The motor angular position and angular velocity can be measured for both the drive and the load side. Both accuracies are $24\,\mathrm{bits}$. It is also possible to specify the torque command value for the load side as well as the drive side. The torque value can be measured by a torque meter (UTM-Ⅲ). The measurement bandwidth is $5\,\mathrm{kHz}$. In this paper, this motor system is modeled as a two-inertia system as shown in a part of Fig. 4(a). The part from the drive-side motor to the input shaft of the strain wave gear is considered the drive side, while the part from the output shaft of the strain wave gear to the load-side motor is considered the load side. The definitions of the plant parameters are shown in Table I.

The frequency response data of the plant from the drive-side torque τ_M to the drive-side angular velocity ω_M, the torsional torque τ_S, and the load-side angular velocity ω_L were obtained with Chirp signals, respectively. The data and the corresponding nominal transfer functions are shown in Fig. 3. The frequencies of the first and most dominant anti-resonance and resonance were observed to be about $14\,\mathrm{Hz}$ and $33\,\mathrm{Hz}$, respectively.

III. Admittance Control

Admittance control is the control of the desired transfer function (admittance) from an external force applied from the environment to the output speed of the plant. If a human applies torque directly to the system from an external source, the system will feel as if it were the desired plant The desired transfer function is, for example, specified with some physical parameters as follows:

$$\frac{\omega}{\tau} = \frac{s}{J_D s^2 + D_D s + K_D}, \tag{1}$$

where J_D, D_D, and K_D denote a desired inertia, a desired viscosity, and a desired stiffness, respectively. The basic admittance control is described. A velocity reference is generated from the external force applied from the environment to achieve the desired admittance. A velocity loop is set to follow the velocity reference.

A. Conventional admittance control for rigid body

In this paper, the system shown in Fig. 4(a) is the conventional method in order to make the comparison with the proposed method described later as fair as possible. A similar system is, for example, used in [18]. With the torque applied by humans τ_L and the desired plant admittance $P_D(s)$, the load-side angular velocity reference ω_L^{ref} is calculated as follows:

$$\omega_L^{ref} = P_D(s)\tau_L. \tag{2}$$

As $P_D(s)$, the following is used:

$$P_D(s) = \frac{1}{J_D s + D_D}, \tag{3}$$

where J_D and D_D denote a desired inertia and a desired viscosity, respectively. The conversion from the load-side angular velocity reference ω_L^{ref} to the drive-side angular velocity reference ω_M^{ref} is done as follows:

$$\omega_M^{ref} = N\omega_L^{ref}. \tag{4}$$

This is the approximation where the plant is regarded as a rigid body. From the above, the transformation from τ_L to ω_M^{ref} is

$$\omega_M^{ref} = P_D(s)N\tau_L. \tag{5}$$

Therefore, $F_{dc}(s)$ in Fig. 4(a) is

$$F_{dc}(s) = P_D(s)N. \tag{6}$$

TABLE I
THE PARAMETERS OF THE CONTROL PLANT.

symbol	parameter	value	unit
J_M	Inertia of the drive-side motor	1.66e-5	$\mathrm{kg\,m^2}$
J_L	Inertia of the load-side motor	1.66e-1	$\mathrm{kg\,m^2}$
D_M	Viscosity coefficient of the drive-side motor	1.5e-3	$\mathrm{N\,m/(rad/s)}$
D_L	Viscosity coefficient of the load-side motor	4.0e-2	$\mathrm{N\,m/(rad/s)}$
K	Stiffness of the strain wave gear	1.68e3	$\mathrm{N\,m/rad}$
N	Reduction ratio of the strain wave gear	50	-

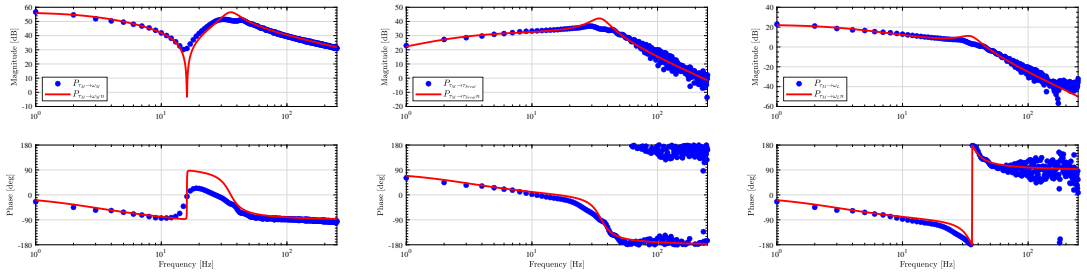

(a) τ_M to ω_M (b) τ_M to τ_S (c) τ_M to ω_L

Fig. 3. Frequency response data from τ_M

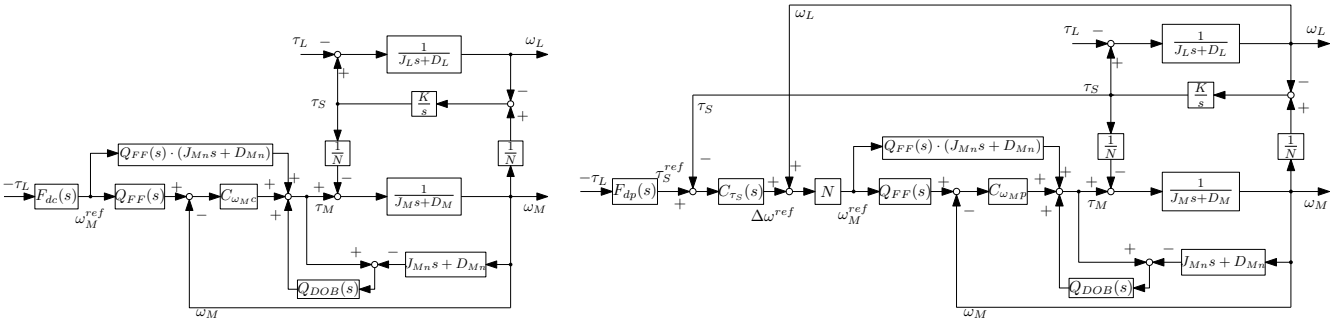

(a) The block diagram of the conventional method. (b) The block diagram of the proposed method.

Fig. 4. The block diagrams of the conventional method and the proposed method.

For the obtained drive-side angular velocity reference ω_M^{ref}, drive-side angular velocity ω_M is controlled. The control system of drive-side angular velocity ω_M is composed of a disturbance observer, a feedback controller, and a feedforward controller. Adding a disturbance observer, the plant for drive-side angular velocity ω_M control is regarded as the single inertia system composed of only the drive side. $Q_{DOB}(s)$ in Fig. 4(a) is the first-order low-pass filter.As the feedback controller, shown as $C_{\omega_M c}$ in Fig. 4(a), the proportional(P) controller is used. The design method is a pole placement method for a drive-side single inertia system. The feedforward controller is designed for a drive-side single inertia system based on 2-DOF control. $Q_{FF}(s)$ in Fig. 4(a) is the first-order low-pass filter.

This control system uses the assumption described above. If the plant were a rigid body, the following equation would hold:

$$\omega_M = N\omega_L. \tag{7}$$

In reality, however, this equation is not valid due to the torsion of the transmission part, angle transmission errors, and so on. This causes the vibration of the whole system, and we cannot regard the plant as the desired plant.

B. Proposed Admittance Control

The proposed admittance control method uses torsional torque control. Let's define the load-side dynamics $P_L(s)$ as $P_L(s) = \frac{1}{J_L s+D_L}$. From the load-side dynamics,

$$P_L(s)(\tau_S - \tau_L) = \omega_L. \tag{8}$$

From the definition of admittance,

$$\frac{\omega_L}{\tau_L} = -P_D(s). \tag{9}$$

Therefore, the following equation holds:

$$\tau_S = \left(\frac{P_D(s)}{P_L(s)} - 1\right)(-\tau_L). \tag{10}$$

This means that when the reference of the torsional torque τ_S is set to the right terms of the equation and the torsional torque

τ_S is controlled to track the reference, the whole system is an admittance control system. In other words, admittance controls can be attributed to the torsional torque control using equation 10. This can take into account two-inertia system dynamics and enables proper the filter to convert $-\tau_L$ into τ_S. The load-side torque τ_L is not a disturbance if the torsional torque τ_S is controlled because the torsional torque τ_S is added as assist torque for the load-side torque τ_L. The filter to convert $-\tau_L$ into τ_S is denoted as follows:

$$F_{dp}(s) = \frac{P_D(s)}{P_L(s)} - 1, \tag{11}$$

which is used in Fig. 4(b).

As torsional torque control, we use a system configuration based on the method of the paper [19]. The block diagram is shown in Fig. 4(b). The torsional torque control mainly consists of an inner loop of ω_M and an outer loop of τ_S. The ω_M inner loop uses a feedforward controller, a disturbance observer, and a feedback controller, shown as $C_{\omega_M p}$ in Fig 4(b). This is the same as described in the conventional method. The outer loop of τ_S makes effective use of ω_L to facilitate feedback design inspired by research that makes effective use of load-side encoders [20]. For the transmission error of angular velocity, the following equation holds:

$$\omega_M = N(\Delta\omega + \omega_L). \tag{12}$$

This means that when $\Delta\omega$ is controlled, we can use ω_L to make the command value of ω_M. Therefore, the transfer function from the angular velocity transmission error $\Delta\omega$ to the torsional torque τ_S is regarded as the control subject for the outer loop. The feedback controller of the outer loop, shown as $C_{\tau_S}(s)$ in Fig. 4(b), is a proportional-integral (PI) controller and the design method is a multiple root pole placement method for the transfer function from $\Delta\omega$ to τ_S, that is $\frac{K}{s}$. Note that although the backlash is compensated in a feed-forward manner in the [19], the reducer used in this study is a harmonic drive with a small backlash, so feed-forward compensation of the backlash is not used in this study.

IV. Simulations

A. Time responses

1) Condition of the simulations: As the parameters of the plant, the parameters shown in Table I were used. The system shown in Fig. 4(a) was used as the conventional method while the system shown in Fig. 4(b) was used as the proposed method. For a fair comparison, the poles of the outer loops of both the conventional method and the proposed method were set to the same value. The poles of the outer loops were set to $5\,\mathrm{Hz}$. The pole of the inner loop of the proposed method was set to $17\,\mathrm{Hz}$. The cutoff frequencies of $Q_{DOB}(s)$ and $Q_{FF}(s)$ were set to $100\,\mathrm{Hz}$. As desired parameters, J_D and D_D were set as $J_D = \frac{1}{30}J_L$, $D_D = 20D_L$. This parameter set was just an example of desired plant parameters. This set meant that control systems performed in the transient response as assistant systems, while performed in the constant response as load-giving systems or systems more likely to stop moving. The load-side torques τ_L was not estimated. For the load-side torques, step inputs applied a low pass filter were used. The constant values of them were $0.56\,\mathrm{N\,m}$, and the cutoff frequencies of the low-pass filters were $100\,\mathrm{Hz}$. The simulations were performed with MATLAB/Simulink®. The calculation periods of the plant and the control systems were set to $0.01\,\mathrm{ms}$. We interpreted these simulations as continuous-time simulations. No perturbation and no nonlinearity were considered. Our goal was to make the plant work as if it were the plant which had desired admittance without vibration of the two-inertia system. The differences between the ω_L in each method and that of the plant which had desired admittance, especially the vibration, were noted.

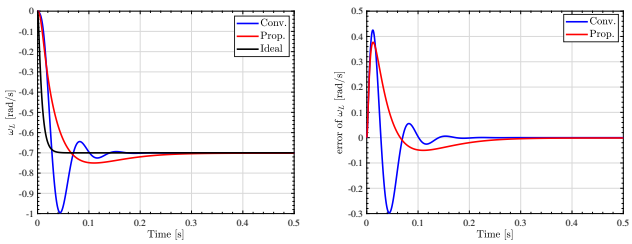

(a) Simulation results of time response of ω_L.

(b) Simulation results of time response of error of ω_L.

Fig. 5. Simulation results of time response."Ideal", "Conv.", and "Prop." denote the response of the desired plant, the response of the conventional method, and the response of the proposed method, respectively.

2) Results of the simulations: The comparison of ω_L in the simulation in the time domain is shown in Fig. 5(a). The comparison of the error of ω_L in each method relative to ω_L in the desired plant in the simulation in the time domain is shown in Fig. 5(b). The response speed of the proposed method was smaller than that of the conventional method. However, there were merits in the proposed method with respect to vibration and overshoot. The conventional method had a large overshoot and vibration in the initial response. On the other hand, the proposed method had a smaller overshoot and seemed to have no vibration. The first overshoot of the conventional method is about $42.2\,\%$. The overshoot of the proposed method is about $7.1\,\%$. Thus, the proposed method could save about $35.1\,\%$. It could also work without vibration occurring in the conventional method.

B. Frequency responses

1) Conditions of the simulations: The parameters of the plant and the control system were the same as that of simulations in time response. We get frequency response data from τ_L to ω_L. The Nyquist diagram is also examined. To get frequency response data, a Chirp signal was input as τ_L and ω_L were observed. The conditions regarding calculations were the same as that of simulations in time response. The frequency response data, especially the properties around anti-resonance frequency is noted. In the Nyquist diagram, phase margins are especially noted.

2) Result of the simulations: The comparison of the frequency response data of the conventional method and the

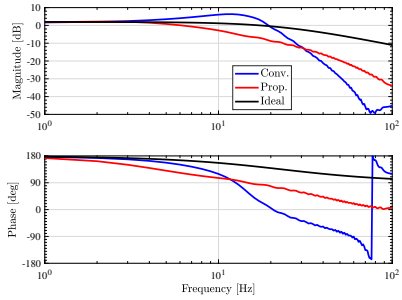

Fig. 6. Simulation results of frequency response from τ_L to ω_L.

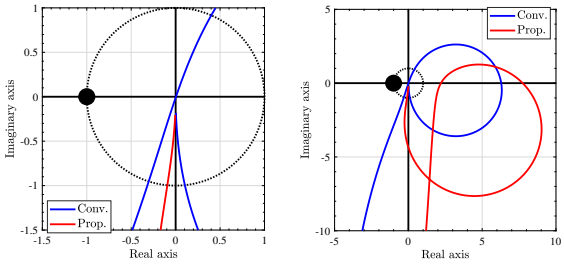

(a) Simulation results of the Nyquist diagram.

(b) Simulation results of the Nyquist diagram (reduced).

Fig. 7. Simulation results of the Nyquist diagram."Conv." and "Prop." denote the response of the conventional method and response of the proposed method, respectively.

proposed method in the simulations are shown in Fig. 6. Around the frequency range from 5 Hz, which is the pole of the outer loops, to 20 Hz, the gain of the conventional method is larger than that of the desired plant. On the other hand, the gain of the proposed method in that range did not exceed that of the desired plant. Considering the pole placement of the outer loops, the gain would reduce from around 5 Hz. Note that the anti-resonance frequency of the plant is about 14 Hz. It would be considered that the conventional method could not suppress the gain excitement because it did not consider the dynamics of the two-inertia system. The proposed method could suppress the gain around anti-resonance frequency because it made the dynamics of the two-inertia system into consideration. The gain was less likely to reduce in the range larger than the anti-resonance frequency in the proposed method than the conventional method.

The comparison of the Nyquist diagrams of the conventional method and the proposed method are shown in Fig. 7. These are the results obtained when the poles of the outer loop of the conventional method and the proposed method are the same. In spite of this fact, the proposed method has a larger phase margin. The reduced Nyquist diagrams as shown in Fig. 7(b) shows the Nyquist locus of the proposed method in the low-frequency range is further from the point -1 than that of the conventional method.

3) Discussion on physical quantities to be fed back: The control systems using the drive-side angular velocity ω_M and the torsional torque τ_S were compared in the simulation

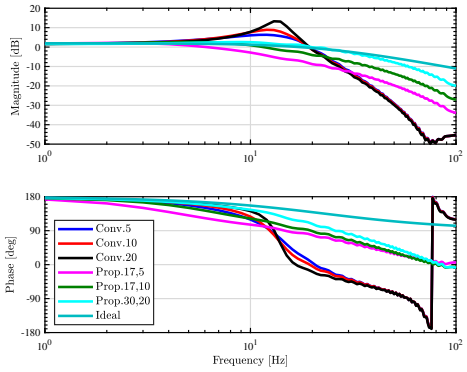

Fig. 8. Simulation results of frequency response from τ_L to ω_L of various poles. The numbers after "Conv.", the numbers right after "Prop." and the second numbers after "Prop." represent the poles of ω_M in the conventional method, those of ω_M in the proposed method, and those of τ_S, respectively.

above. Now assume each control is perfect, that is the transfer function from the reference to real value is 1. Then, admittance performance is considered to be determined by the transfer function from that real value to the load-side angular velocity ω_L. The transfer function from ω_M to ω_L is shown as follows:

$$G_{\omega_L\omega_M} = \frac{J_D s^2 + D_D s + K}{N(J_L s^2 + D_L s + K)}, \tag{13}$$

where $G_{\omega_L\omega_M}$ means transfer function from ω_M to ω_L. In the case of the admittance control based on τ_S feedback, however, the whole system is strictly identical to the desired admittance without the excitement of the gain when the plant is nominal. Even if the controls are perfect, the admittance control based on ω_M feedback vibrates at the resonance frequency, while τ_S does not have that defect. To back up the theory, the frequency response data of various poles of the conventional method and the proposed method are shown in Fig. 8. This shows the gain of the conventional method at the anti-resonance of the plant increase as the pole gets large while that of the proposed method does not increase. Admittance control using the torsional torque feedback enables higher control bandwidth than the conventional method. Note that the control of ω_L is not discussed here because the bandwidth cannot be increased due to the phase delay.

V. Experiments

The experiments were performed on time responses.

A. Conditions of the experiments

Structures of systems used as a conventional method and a proposed method were the same as that of the simulations. The design parameters of the control systems were the same as that of the simulations. The calculation period of the control systems and the sampling period of the sensing of the physical quantities used for the controls were set to 500 µs. The discretization method was the Tustin transform. The load-side torque τ_L were not estimated. The parameters of the load-side τ_L as human torque were the same as the simulations. The control systems were implemented with YASKAWA software.

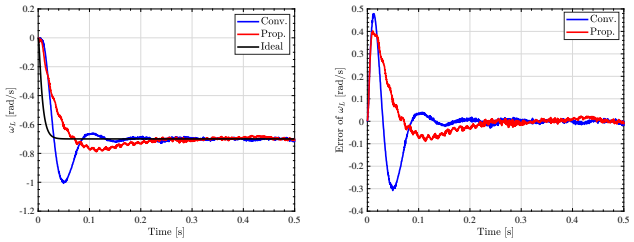

(a) Experimental results of time response of ω_L.

(b) Experimental results of time response of error of ω_L.

Fig. 9. Experimental results of time response."Ideal", "Conv.", and "Prop." denote response of the desired plant, response of the conventional method and response of the proposed method, respectively.

We observed the differences between the ω_L in each method and that of the plant which has desired admittance, especially the vibration.

B. Results of the experiments

The comparison of ω_L in the simulation in the time domain is shown in Fig. 9(a). As the simulations, it was observed that the proposed method was prior to the conventional method in the vibration due to the anti-resonance of the plant. The first overshoot of the conventional method is about $43.9\,\%$. The overshoot of the proposed method is about $12.8\,\%$. Thus, the proposed method could save about $31.1\,\%$. It could also work without vibration due to the anti-resonance of the plant occurring in the conventional method.

VI. Conclusion & Future work

There is an increasing need for collaborative robots. We designed the control system so that the whole system does not vibrate at the anti-resonance frequency of the plant. The admittance control was attributed to the torsional torque control. The simulations and experimental results show the effectiveness of the proposed method in vibration at the first anti-resonance frequency. However, the proposed method is vulnerable to the uncertainty of the load-side plant parameters. The future work is to make the system robust to the load-side plant parameters.

Acknowledgment

This work was partially supported by Tsugawa Foundation.

References

[1] L. Gualtieri, E. Rauch, and R. Vidoni, "Emerging research fields in safety and ergonomics in industrial collaborative robotics: A systematic literature review," *Robotics and Computer-Integrated Manufacturing*, vol. 67, no. July 2019, 2021. [Online]. Available: https://doi.org/10.1016/j.rcim.2020.101998

[2] E. Dunwoodie, R. Mutlu, B. Ugurlu, M. Yildirim, T. Uzunovic, and E. Sariyildiz, "A High-Torque Density Compliant Actuator Design for Physical Robot Environment Interaction," pp. 1–6, 2020.

[3] T. Nef and P. Lum, "Improving backdrivability in geared rehabilitation robots," *Medical & biological engineering & computing*, vol. 47, no. 4, pp. 441–447, 2009.

[4] M. J. Kim, F. Beck, C. Ott, and A. Albu-Schäffer, "Model-Free Friction Observers for Flexible Joint Robots with Torque Measurements," *IEEE Transactions on Robotics*, vol. 35, no. 6, pp. 1508–1515, 2019.

[5] S. Suzuki, Y. Kawai, Y. Yokokura, K. Ohishi, T. Miyazaki, and T. Shinozaki, "Single-Inertialization Based on High-Backdrivability Control Using Equivalent Disturbance Compensator for Human Interaction Robot," *IEEJ Journal of Industry Applications*, vol. 10, pp. 282–291, 2021.

[6] A. Hasegawa, H. Fujimoto, and T. Takahashi, "Filtered disturbance observer for high backdrivable robot joint," in *IECON 2018-44th Annual Conference of the IEEE Industrial Electronics Society*. IEEE, 2018, pp. 5086–5091.

[7] S. Yamada and H. Fujimoto, "Position-based High Backdrivable Control Using Load-side Encoder and Backlash," *IEEJ Journal of Industry Applications*, vol. 10, pp. 142–152, 2020.

[8] S. Xu, M. Yokoyama, and T. Shimono, "Back-drivability improvement of geared system based on disturbance observer and load-side disturbance observer," *IEEJ Journal of Industry Applications*, vol. 9, no. 5, pp. 475–485, 2020.

[9] K. Nagano, T. Shimono, and Y. Fujimoto, "Backdrivability Improvement Method Based on Angular Transmission Error in a High Reduction Gear," *IEEJ Journal of Industry Applications*, vol. 8, no. 5, pp. 779–786, 2019.

[10] N. Hogan, "Impedance control: An approach to manipulation: Part i-theory," 1985.

[11] G. Kang, H. S. Oh, J. K. Seo, U. Kim, and H. R. Choi, "Variable Admittance Control of Robot Manipulators Based on Human Intention," *IEEE/ASME Transactions on Mechatronics*, vol. 24, no. 3, pp. 1023–1032, 2019.

[12] Y. M. Hamad, Y. Aydin, and C. Basdogan, "Adaptive Human Force Scaling via Admittance Control for Physical Human-Robot Interaction," *IEEE Transactions on Haptics*, vol. 14, no. 4, pp. 750–761, 2021.

[13] I. Ranatunga, F. L. Lewis, D. O. Popa, and S. M. Tousif, "Adaptive Admittance Control for Human-Robot Interaction Using Model Reference Design and Adaptive Inverse Filtering," *IEEE Transactions on Control Systems Technology*, vol. 25, no. 1, pp. 278–285, 2017.

[14] C. Yang, G. Peng, L. Cheng, J. Na, and Z. Li, "Force Sensorless Admittance Control for Teleoperation of Uncertain Robot Manipulator Using Neural Networks," *IEEE Transactions on Systems, Man, and Cybernetics: Systems*, vol. 51, no. 5, pp. 3282–3292, 2021.

[15] A. Q. Keemink, H. van der Kooij, and A. H. Stienen, "Admittance control for physical human-robot interaction," *International Journal of Robotics Research*, vol. 37, no. 11, pp. 1421–1444, 2018.

[16] S. P. Buerger and N. Hogan, "Complementary stability and loop shaping for improved human-robot interaction," *IEEE Transactions on Robotics*, vol. 23, no. 2, pp. 232–244, 2007.

[17] B. Lacevic and P. Rocco, "Closed-form solution to controller design for human-robot interaction," *Journal of Dynamic Systems, Measurement and Control, Transactions of the ASME*, vol. 133, no. 2, pp. 1–7, 2011.

[18] Y. Asai, Y. Yokokura, and K. Ohishi, "Mechanical admittance realization control based on feedforward compensation for fine realization of impedance," *IEEJ Journal of Industry Applications*, vol. 6, no. 2, pp. 83–90, 2017.

[19] S. Yamada and H. Fujimoto, "Precise joint torque control method for two-inertia system with backlash using load-side encoder," *IEEJ Journal of Industry Applications*, vol. 8, no. 1, pp. 75–83, 2019.

[20] K. Sakata, H. Asaumi, K. Hirachi, K. Saiki, and H. Fujimoto, "Self resonance cancellation techniques for a two-mass system and its application to a large-scale stage," *IEEJ Journal of Industry Applications*, vol. 3, no. 6, pp. 455–462, 2014.